# Geostrophically Constrained Flow of Warm Subsurface Waters Into Geometrically Complex Ice Shelf Cavities

**G. Finucane[1] and A. L. Stewart[1]**

[1]Department of Atmospheric and Oceanic Sciences, University of California, Los Angeles, California, USA

**Key Points:**

- We introduce a new theoretical framework for inflow of warm water into ice shelf cavities based on geostrophically-constrained circulation.
- A new metric, the Highest Unconnected Isobath (HUB), quantifies bathymetric barriers to warm water access in complex geometries.
- Our HUB-informed theoretical framework is able to accurately predict melt rates across a suite of idealized models and in observational data.

Corresponding author: Garrett Finucane, `gdf@ucla.edu`

**Abstract**

Antarctic ice shelves are losing mass at drastically different rates, primarily due to melting by relatively warm Circumpolar Deep Water (CDW). Previous studies have identified seafloor bathymetry as a key obstacle to CDW intrusions across the continental shelf and beneath ice shelves, but a generalized theory for geometrically-influenced ice melt is lacking. This study proposes such a theory based on geostrophically-constrained CDW inflow, combined with a threshold bathymetric elevation that obstructs CDW access to ice shelf grounding lines, referred to as the Highest Unconnected isoBath (HUB). This theory captures 90% of the variance in melt rates across a suite of process-oriented ocean/ice shelf simulations with various quasi-randomized geometries. Applied to observed ice shelf geometries and offshore hydrography, the theory captures $>80\%$ of the variance in measured ice shelf melt rates. These findings provide a generalized theoretical framework for melt resulting from buoyancy-driven CDW access to geometrically complex Antarctic ice shelf cavities.

## Plain Language Summary

The floating extensions of Antarctic glaciers ("ice shelves") are losing ice at drastically different rates. A large component of this ice loss is due to melting from below by relatively warm ocean waters, which typically lie hundreds of meters below the surface. Previous studies have attempted to derive generalized relationships between oceanic conditions and rates of ice shelf melt. However, these relationships struggle to capture the variations in ice shelf melt around Antarctica, in part because but they do not account for obstruction of warm water access by complex variations in the shape of the seafloor. In this study we introduce a new theory for the rate at which warm waters access Antarctica's ice shelves. This theory is grounded in the assumption that the ocean flow beneath cavities is dominated by the rotation of the earth, and utilizes a novel quantification of seafloor obstruction of warm water inflows. We show that this theory is successful at predicting melt in computer simulations of ice shelves of different shapes, and in observations of real ice shelves. This work provides a general theoretical grounding for melt resulting from warm subsurface waters flowing underneath Antarctic ice shelves.

## 1 Introduction

The mass loss of Antarctic ice shelves has been accelerating for the past four decades (Paolo et al., 2015; Shepherd et al., 2018). This mass loss has been attributed to the basal melt on the underside of floating ice shelves, which is driven by oceanic heat fluxes (Shepherd et al., 2004; Pritchard et al., 2012). The most vigorous basal melt in the Antarctic comes from the intrusion of a subsurface warm water mass called Circumpolar Deep Water (CDW) into ice shelf cavities (Jacobs et al., 1996; Jenkins et al., 2010; Nakayama et al., 2019; Rignot et al., 2019). The depth and temperature of CDW vary around Antarctica (Schmidtko et al., 2014). Ice shelves with shallower CDW and deep troughs tend to have higher melt (Nitsche et al., 2017). Fig. 1 illustrates this point via the temperature offshore at 500m depth, the depth of the continental shelf at locations shallower than 500m, and ice shelf melt rates from Adusumilli et al. (2020).

There are various controls on the supply of CDW from the open ocean to the continental shelf. Wind stresses over the continental slope lead to cross-slope Ekman transport that has been linked to variability of CDW heat fluxes across and along the shelf in observations (Assmann et al., 2013) and models (Spence et al., 2014; Thoma et al., 2008; Dotto et al., 2020; Tamsitt et al., 2021). Wind forcing over the continental shelf can also lead to vigorous deep mixing which erodes the thickness of CDW on the shelf (Caillet et al., 2023; Moorman et al., 2023). Surface buoyancy losses, for example due to sea ice formation in coastal polynyas, are also able to erode the thickness of CDW across the shelf by deepening the mixed layer (Webber et al., 2017; Caillet et al., 2023). In some

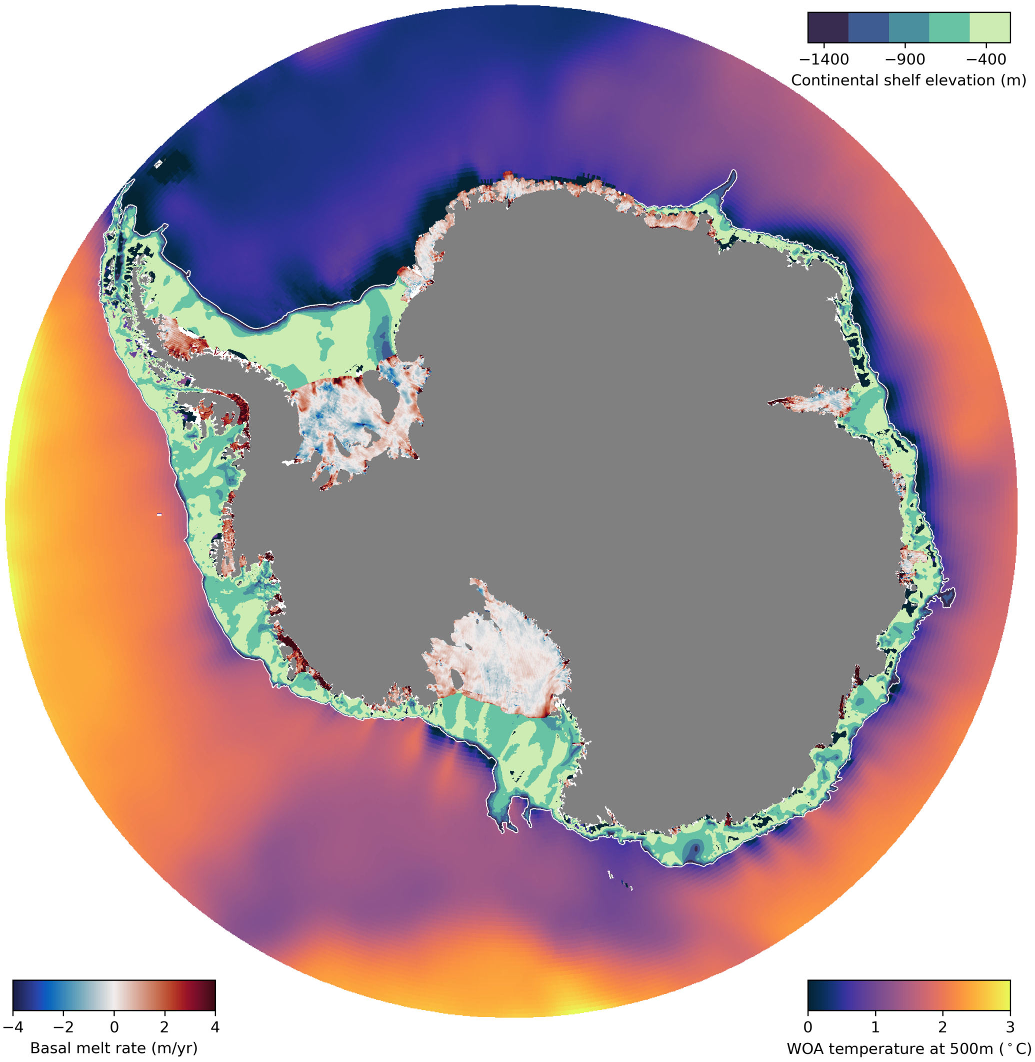


**Figure 1.** World Ocean Atlas (Boyer et al., 2018) temperatures at a depth of 500m are plotted for locations with a depth greater than 1500m. The bathymetry of the continental shelf from BedMachine2 (Morlighem, 2020) is plotted for depths shallower than 1500m in regions that are not covered by ice shelves. Where there are ice shelves, the satellite derived basal melt rate from Adusumilli et al. (2020) is plotted.

regions these polynyas produce High Salinity Shelf Water (Nicholls et al., 2009) that fills the ice shelf cavities, blocking the intrusion of CDW (Hellmer et al., 2017; Hazel & Stewart, 2020). In other regions, precipitation onto the ocean in front of the ice shelves can enhance stratification and lead to more lateral transport of CDW to ice shelf faces (Flexas et al., 2022).

Among the various influences on CDW intrusions, previous studies have consistently emphasized the role of bathymetry (Klinck & Dinniman, 2010; Heimbach & Losch, 2012; Nakayama et al., 2019). In particular, deep troughs have been shown to allow CDW to flow mostly unimpeded from offshore into ice shelf cavities in models (Schodlok et al., 2012; St-Laurent et al., 2013; Haigh et al., 2023) and in observations (Assmann et al., 2013; Rintoul et al., 2016). Modeling studies have similarly shown that raising CDW above the height of the main bathymetric obstacles is a necessary condition for pushing cold shelves like the Filchner-Ronne from a low-melt state to a high-melt state (Daae et al., 2020; Hazel & Stewart, 2020).

While many previous studies have offered insight into the dynamics of the circulation of CDW in ice shelf cavities and the resulting melt, there is still a need for parameterizations and theories that accurately encapsulate the salient influences on CDW inflow and melt. Previous studies have found the circulation inside the cavity itself is buoyancy-driven (Walker et al., 2007; Wåhlin et al., 2010; De Rydt et al., 2014; Morrison et al., 2020; Zhao et al., 2019). There have been attempts to link the net melt rate of ice shelves to the bulk properties of the CDW layer and ice shelf cavity geometry (Holland et al., 2008; Little et al., 2009; Lazeroms et al., 2018). Burgard et al. (2022) evaluated existing basal melt parameterizations in a regional model that included ice shelves and found that the parameterizations error was often on the order of the signal. Lazeroms et al. (2018) found that a plume-based melt parameterization could approximately replicate the observed spatial patterns of ice shelf melt, but only with the aid of a tuning parameter that was specific to each ice shelf. Thus it remains unclear to what extent the buoyancy-driven circulation theory extends outside the cavity to the circulation across the continental shelf, and if it generalizes to geometrically complex continental shelves and ice shelf cavities.

In this study we will present a new dynamical framework which determines heat flux into ice shelf cavities based on a geostrophic constraint on the CDW transport (Section 2). This allows us to predict the average ice shelf melt rate from the hydrographic conditions outside of an ice shelf cavity. We combine this theory with a novel quantification of the bathymetric obstruction of CDW access, referred to as the Highest Unconnected isoBath (HUB, Section 3). We then test our theory against a suite of idealized models simulations (Section 4) and against observed ice shelf melt rates (Section 5).

## 2 Geostrophically constrained CDW heat flux into ice shelf cavities

In this section we will formulate a theoretical framework for estimating ice shelf cavity melt based on the external hydrography and cavity geometry. Our theory is grounded in the same physical principle as that of Zhao et al. (2019): that the geostrophic transport of CDW parallel to the grounding line is redirected inwards into the cavity by a boundary current, and thus is directly related to the heat transport toward the grounding line. This is analogous to previous scaling theories for buoyancy-driven circulation in enclosed basins in the open ocean (Gnanadesikan, 1999; Nikurashin & Vallis, 2012; Youngs et al., 2020). Our theory contrasts with previous parameterizations (e.g. Holland et al., 2008; Lazeroms et al., 2018; Pelle et al., 2019) based on processes occurring in the ice-ocean boundary layer; this is discussed further in Section 6.

To formulate our theory, we idealize the ice shelf cavity circulation as a two-layer flow, comprised of fresh cold layer overlying above a warm salty layer (Fig. 2(b)). As-

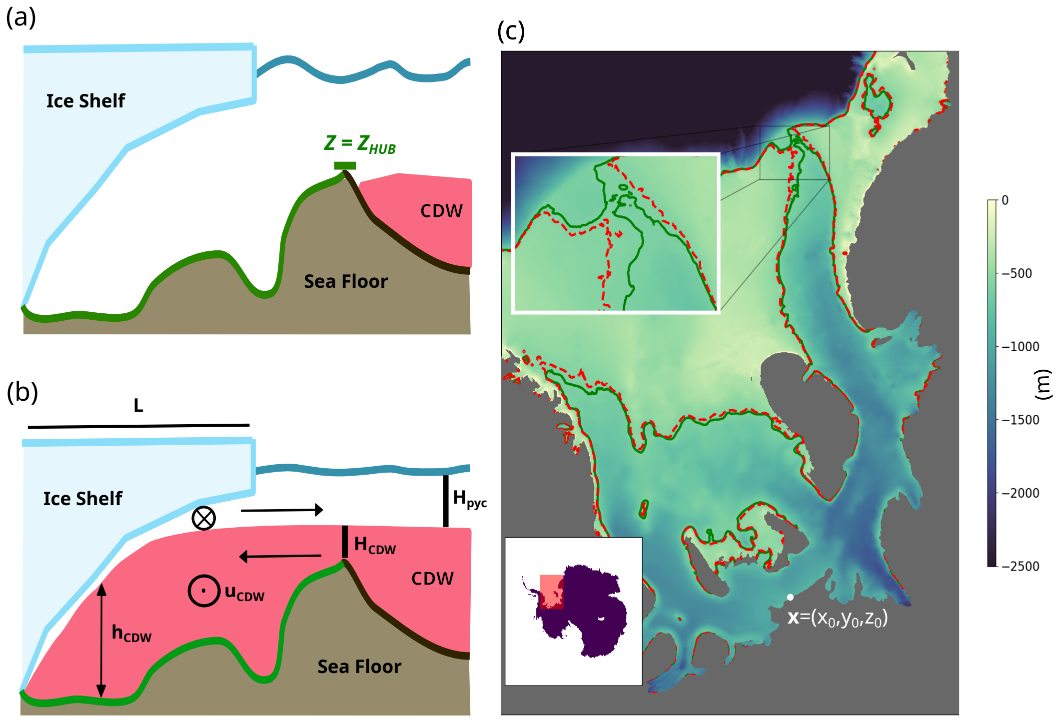


**Figure 2.** (a) A schematic representation of the highest unconnected isobath (HUB; see Section 3) in two dimensions. All points colored green underneath the ice shelf colored share the same HUB depth of $z_{\mathrm{HUB}}$; we posit that CDW must be shallower than this in order to access the region indicated by the green curve along the seafloor, and thus melt the ice shelf. (b) An illustration of the proposed watermass structure which is assumed by the theory presented in 2. (c) A map of the bathymetry of the Filchner-Ronne ice shelf (FRIS). Regions with grounded ice are filled in black. The green contour (z=-605m) is closed, meaning that for water from the open ocean to reach grounding line points at the southern end of the FRIS, they must rise shallower than z=-605m. The red contour (z=-600m) is open, meaning that this is the shallowest depth that CDW must reach in order to access the southern grounding line points of the FRIS. This means the HUB depth for the FRIS is z=-600m (note that the resolution of our HUB depth calculation is 5m).

suming vertically uniform flow in each layer, the cross-cavity geostrophic flow of CDW may then be formulated as

$$T = \int \mathrm{d}y\, u_{\mathrm{CDW}} h_{\mathrm{CDW}} \sim \int \mathrm{d}y\, \frac{g'_{\mathrm{in}}}{f} s_{\mathrm{CDW}} h_{\mathrm{CDW}}, \tag{1}$$

where $y$ is an along-cavity coordinate, $h_{\mathrm{CDW}}$ is the thickness of the CDW layer, and $u_{\mathrm{CDW}}$ is the cross-cavity CDW velocity. Here we have scaled the cross-cavity flow by the geostrophic shear, i.e. $u_{\mathrm{CDW}} \sim (g'_{\mathrm{in}}/|f|)s_{\mathrm{CDW}}$, where $s_{\mathrm{CDW}}$ is the slope of the isopycnal interface between CDW and the overlying waters, $f$ is the Coriolis parameter, and $g'_{\mathrm{in}} = g(\sigma_{\mathrm{CDW}} - \sigma_{\mathrm{surf}})/\rho_0$ is the reduced gravity. To further simplify (1) we assume that the interface between the two density layers approximately follows the shape of the ice draft, i.e. $s_{\mathrm{CDW}} \sim s_{\mathrm{ice}}$, due to melting and mixing processes at the ice-ocean boundary (see Fig. 2a and Section 4). Taking $L$ to be a representative distance from the grounding line to the ice front, we scale (1) as

$$T \sim \frac{g'_{\mathrm{in}}}{|f|} s_{\mathrm{ice}} H_{\mathrm{CDW}} L. \tag{2}$$

Here $H_{\mathrm{CDW}}$ is a representative CDW layer thickness, which we assume to be constrained by bathymetry between the grounding line and the continental shelf break (see Fig. 2 and Section 3).

To estimate the amount of melt which occurs due to this inflow of CDW, we assume (i) that the net transport of CDW into the cavity is balanced by return flow of freezing-temperature meltwater, and (ii) that the net advective heat transport into the cavity is balanced by heat lost to the ice shelf via melting. The latter assumption holds provided that the cavity is in steady state, i.e., over time scales much longer than the cavity flushing time scale (Holland, 2017). This heat balance can be expressed as

$$\rho_{\mathrm{i}} I_{\mathrm{f}}\, \dot{m} W L \sim \rho_0 C_{\mathrm{p}} T (\theta_{\mathrm{CDW}} - \theta_{\mathrm{surf}}) \tag{3}$$

where $W$ is the cross-cavity width, $\dot{m}$ is the melt rate per unit area, $C_{\mathrm{p}}$ is the specific heat capacity of seawater, $\rho_0$ is a reference ocean density, $\rho_{\mathrm{i}}$ is the reference density of ice, $I_{\mathrm{f}}$ is the latent heat of melting, $\theta_{\mathrm{CDW}}$ is the temperature of the CDW, and $\theta_{\mathrm{surf}}$ is the surface freezing temperature. Substituting (1) into (3) and rearranging leads to the following scaling for the area-averaged melt rate,

$$\dot{m}_{\mathrm{pred}} \equiv \frac{\alpha g'_{\mathrm{in}} \rho_0 C_{\mathrm{p}}}{|f| \rho_{\mathrm{i}} I_{\mathrm{f}} W} s_{\mathrm{ice}} H_{\mathrm{CDW}} (\theta_{\mathrm{CDW}} - \theta_{\mathrm{surf}}), \tag{4}$$

where $\alpha$ is a non-dimensional scaling parameter.

A shortcoming of this scaling is that in cavities with realistic geometries, the length $L$ and width $W$ are ambiguous. However, in our model simulations (in which the ice shelf cavity does have well-defined dimensions; see Section 4) we find that the stratification in the interior of the cavity varies approximately linearly with width, i.e. $g'_{\mathrm{in}}/W \sim g'_{\mathrm{out}}/W_0$, where $W_0 \approx 100\,\mathrm{km}$ is a constant reference width and $g'_{\mathrm{out}}$ is the reduced gravity outside the cavity. This relationship yields a predicted area-averaged melt rate that is independent of both the cavity width and length, consistent with the findings of Little et al. (2009),

$$\dot{m}_{\mathrm{pred}} = \frac{\alpha g'_{\mathrm{out}} \rho_0 C_{\mathrm{p}}}{|f| \rho_{\mathrm{i}} I_{\mathrm{f}} W_0} s_{\mathrm{ice}} H_{\mathrm{CDW}} (\theta_{\mathrm{CDW}} - \theta_{\mathrm{surf}}) = \mathcal{C} H_{\mathrm{CDW}} \frac{g'_{\mathrm{out}} s_{\mathrm{ice}}}{|f|} (\theta_{\mathrm{CDW}} - \theta_{\mathrm{surf}}). \tag{5}$$

In the last equality of (5) we have contracted all constant parameters into a single constant of proportionality $\mathcal{C}$. Note that Eq. (5) relates the area-averaged melt rate to quantities derived either from the stratification external to the cavity ($\theta_{\mathrm{CDW}} - \theta_{\mathrm{surf}}$, $g'_{\mathrm{out}}$), the geometry of the cavity ($s_{\mathrm{ice}}$) or a combination of the two ($H_{\mathrm{CDW}}$), and thus serves as our theory for ice shelf melt rates.

## 3 Quantifying bathymetric obstructions to CDW inflows: the Highest Unconnected isoBath (HUB)

To apply our theory from the previous section in three dimensions we must calculate the thickness of the CDW layer ($H_{CDW}$), and the temperature of the CDW ($\theta_{CDW}$) at the entrance of the cavity in complex three-dimensional geometries. Because previous studies have shown that the deepest entry points to ice shelf cavities play an important role in transporting heat (e.g. Walker et al., 2007; St-Laurent et al., 2013), it is crucial that our estimates of CDW thickness and temperature account for these deepest entry points.

To generalize this concept across all Antarctic ice shelves, we formulate a new metric called the Highest Unconnected isoBath (HUB), which may be defined for any reference location on the continental shelf. Conceptually, the HUB may be understood as follows: Consider an ocean that is completely drained of its water, and then slowly fills from its deepest point in such a way that the water is always approximately stationary and in gravitational equilibrium. For any given reference location on the continental shelf, the HUB is defined as the elevation that the water must rise to in order for the reference location to be immersed. This can be captured in a precise topological definition which we provide in the Supporting Information.

Fig. 2(a) provides a two-dimensional visualization of the HUB concept. In this example, all points along the continental shelf highlighted in green share the same HUB, corresponding to the elevation $z_{\mathrm{HUB}}$. That is, CDW must rise to an elevation of at least $z_{\mathrm{HUB}}$ in order to reach any of the points highlighted in green. For a real world example, we return to the case of the Filchner-Ronne ice shelf; Fig. 2(c) shows the HUB for a reference location situated at the ice shelf grounding line. This reference location has a HUB of around 600m, which means that CDW would need rise to an elevation of at least 600m in order to reach the reference location from offshore.

## 4 Predicting melt in idealized ice shelf cavity simulations

To test our theory for the warm water inflow (Section 2), we conduct idealized ocean-ice shelf simulations of warm water inflows that span a wide range of cavity geometries and offshore hydrographies (see Fig. 3). Our simulations utilize the MIT general circulation model (Marshall, Adcroft, et al., 1997; Marshall, Hill, et al., 1997) to evolve the state and circulation of the ocean resulting from the the ocean's thermodynamic and mechanical interactions with a static ice shelf (Losch, 2008). To focus on the buoyancy-driven inflow of CDW, we omit other drivers of ocean circulation such as sea ice, tides, and atmospheric forcing. Instead, we prescribe an analytical profile of potential temperature and salinity at the northern and eastern boundaries of the model domain (see Fig. 3(b) and the Supporting Information), motivated by climatological observations around Antarctica (Boyer et al., 2018).

We illustrate the geometry and forcing of a selected reference case in Fig. 3(a). In this case the ice shelf has geometric dimensions resembling ice shelves in the Amundsen Sea embayment (Morlighem, 2020), being approximately 150km long and 100km wide, with an ice front depth of 250m and a grounding line depth of 1000m. The ice shelf slope is linear, and equal to $s_{ice} = 0.005$ in the reference case. The ice shelf is set in an idealized bathymetric embayment adjacent to an idealized continental slope. For all cases but the reference case we add pseudo-random noise to the shape of the sea floor, with a peak wavelength of 62.5km that is similar magnitude to the width of troughs in the Amundsen (Walker et al., 2007; Dinniman et al., 2011). The random noise is scaled by the water column height (before the random noise is applied) in order to prevent the bathymetric variations from closing off the grounding line. In our reference case, the HUB is approximately 480m.

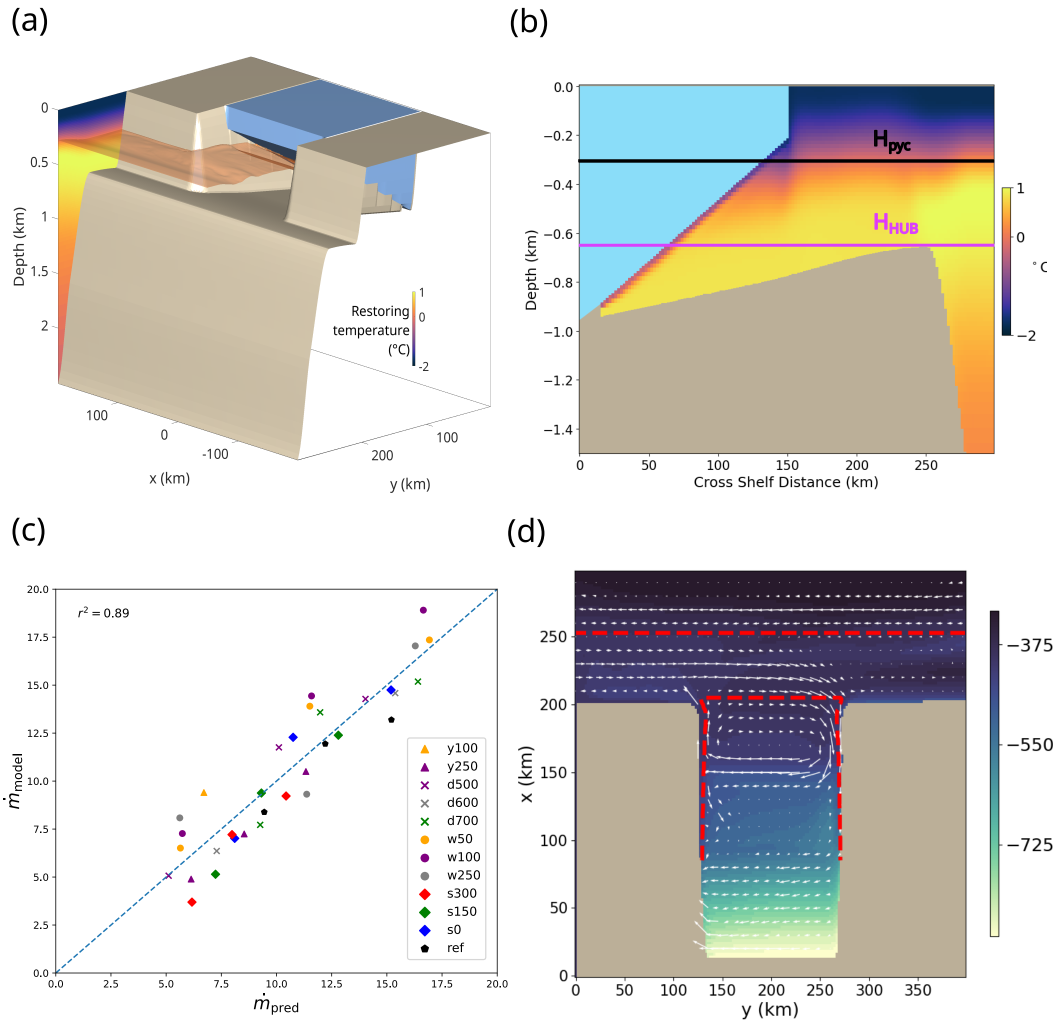


**Figure 3.** (a) Reference run (ref) model geometry with bathymetry in brown, shelf ice in blue, and boundary thermal forcing colored along the eastern edge of the model domain. (b) Time average cross section of temperature from model run in the same geometry. (c) Linear regression of predicted melts from Eq. 5 against diagnosed area- and time-averaged melt rates across out suite of model simulations. Experiments with the same marker and color have the same model geometry, but varying offshore CDW depths. (d) Depth of 0.5 °C isotherm is plotted in the background with white arrows denoting the time average horizontal velocity on that isotherm. The HUB corresponding to the grounding line of this model geometry is shown in red dotted line.

We conduct a series of experiments with different ice shelf/bathymetric geometries by varying the continental shelf slope, the ice shelf slope, the cavity width and the extent of the ice shelf front. A full list of the model geometries used in this study is given in the Supporting Information. For each different ice shelf geometry, we conduct three simulations in which we vary the depth of the subsurface temperature maximum such that it lies 300m deeper than, at the same depth as, and 125m shallower than the HUB. In all experiments we use a horizontal grid spacing of 2km horizontal to ensure adequate resolution of mesoscale eddies (St-Laurent et al., 2013; Stewart & Thompson, 2016), although inspection of the instantaneous flow fields suggests that the flow is not in a strongly eddying regime. We use a vertical grid consisting of 91 geopotential levels, with spacings varying smoothly from 2m at the surface to 200m at the sea floor, with a vertical spacing of approximately 20m at the depth of the ice shelf grounding line (De Rydt et al., 2014). All simulations reach a quasi-steady state by 2.5 years of integration, and are then run for a further 7.5 years for analysis.

We calculate the geostrophically-constrained inflow Eq. 5 in each simulation using the parameters that define the model's offshore hydrography and cavity geometry. We calculate $H_{\mathrm{CDW}}$ by subtracting the HUB from the elevation of the pycnocline depth. The ice slope $s_{\mathrm{ice}}$ is a determined by depth of the ice shelf front, the grounding line depth and the ice shelf front extent. We define the CDW temperature $\theta_{\mathrm{CDW}}$ as the temperature on our prescribed offshore hydrographic profile at the depth of the HUB. Finally, we determine the coefficient $\mathcal{C}$ (and thus $\alpha$) via linear regression using the diagnosed area-averaged melt rates across our entire suite of simulations. This yields $\alpha = 0.29$.

To evaluate our theory, we compare the predicted ($\dot{m}_{\mathrm{pred}}$) and diagnosed ($\dot{m}_{\mathrm{model}}$) area-averaged ice shelf melt rates in Fig. 5(c). We find that the predicted melt rate explains $\sim 90\%$ of the variance in melt rate as diagnosed by the model. Experiments with the same geometry (which have the same marker shape/color in Fig. 5(c)) exhibit increasing predicted and diagnosed melt rates in simulations with higher offshore CDW. This indicates that our theory is successfully capturing the leading order dynamics of warm water inflows in this idealized model.

## 5 Predicting observed ice shelf melt rates

The parameterization from Section 2 is able to accurately predict melt in a geometrically simple model designed to isolate the dynamics of warm water inflows (Section 4). We now formulate and test our theoretical prediction of warm water inflows and melt in observed shelf cavity environments. We draw on observations of near-Antarctic hydrography, as sythesized in the World Ocean Atlas 2018 (Boyer et al., 2018) annual climatology, and on satellite-derived estimates of ice shelf melt from Adusumilli et al. (2020).

The theory encapsulated by Eq. (5) assumes a simplified geometry that contrasts with the complex geometries of natural ice shelf cavities; for example, the depth of real ice shelf grounding lines vary spatially, as does the slope of the ice. In order to generalize the theory to real ice shelf cavity geometries, we compute bulk estimates of the different parameters in our theory (5). Specifically, for a given ice shelf we identify all points from Bedmachine's (Morlighem, 2020) 500m resolution grid which contain grounded ice and are adjacent to floating ice as grounding line points, and then estimate the hydrographic parameters $H_{\mathrm{CDW}}$, $g'_{\mathrm{out}}$ and $\theta_{\mathrm{CDW}} - \theta_{\mathrm{surf}}$ for each grounding line point. We then average those parameters separately over the grounding line to formulate our prediction of the area-averaged melt rate,

$$\dot{m}_{\mathrm{pred}} \equiv \mathcal{C} \langle H_{\mathrm{CDW}} \rangle \overline{s_{\mathrm{ice}}} \langle g'_{\mathrm{out}} \rangle \langle f^{-1} \rangle \langle \theta_{\mathrm{CDW}} - \theta_{\mathrm{surf}} \rangle, \tag{6}$$

where $\langle \cdot \rangle$ denotes an average over all grounding line points within the ice shelf. We treat the ice shelf slope $s_{\mathrm{ice}}$ differently because this parameter is related to the geometry of

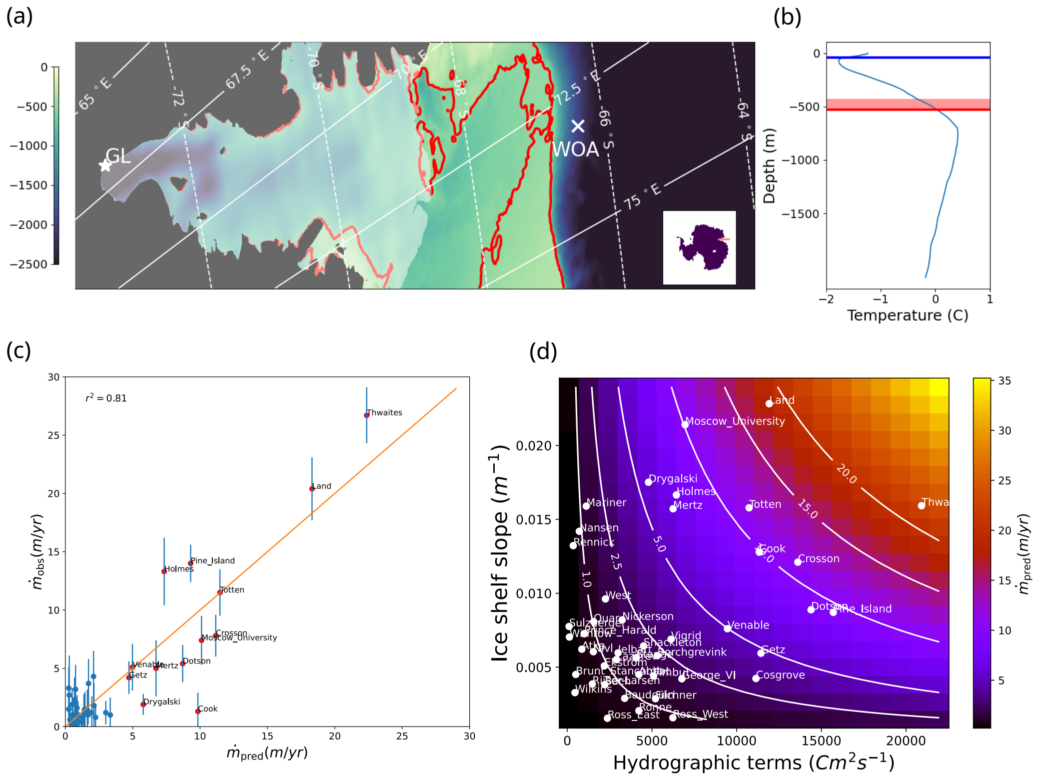


**Figure 4.** Application of our theory to predict circum-Antarctic ice shelf melt rates. (a) An illustration of the off-shore hydrographic cast selection methodology for a single point on the Amery ice shelf grounding line. The bathymetry of the Amery Ice shelf is contoured in blue and green, with floating shelf ice highlighted in white and grounded ice sheet colored dark gray. The red line depicts the HUB depth for the starred grounding line point (GL). The World Ocean Atlas hydrographic cast that is used to estimate heat transport toward point "GL" is labeled "WOA", and is selected as decribed in Section 5. (b) The hydrography at the point labelled "WOA" in panel (a), with the HUB for point "GL" marked by a red line. (c) The linear regression of predicted melt rate from Eq. 5 against observed melt rates from Adusumilli et al. (2020). Error bars are estimates of observational error from Adusumilli et al. (2020). (d) Predicted melt rate (colors and white contours) a function of different parameters in our theory (Eq. 6): the grounding line-averaged hydrographic terms, $\langle H_{\mathrm{CDW}}\rangle\langle g'_{\mathrm{out}}\rangle\langle\theta_{\mathrm{CDW}} - \theta_{\mathrm{surf}}\rangle$, and the cavity-averaged ice shelf slope $\overline{s_{\mathrm{ice}}}$. The corresponding locations in this parameter space of each observed Antarctic ice shelf are indicated by white circles.

the cavity, rather than external hydrographic properties. The overbar $\bar{\cdot}$ denotes an average over the whole ice shelf area, defined more precisely below. The Supporting Information specifies how we choose an appropriate offshore hydrographic cast for each grounding line point, how we calculate the temperature of the CDW layer ($\theta_{\mathrm{CDW}}$), thickness of the CDW layer ($H_{\mathrm{CDW}}$), and exterior reduced gravity ($g'_{\mathrm{CDW}}$), and how we compute the bulk ice shelf slope $s_{\mathrm{ice}}$.

In Fig. 4(c) we compare the melt predicted by our theory (6) against the satellite-derived estimates of basal melt and accompanying uncertainty from Adusumilli et al. (2020). We determine the constant prefactor $\mathcal{C}$ via linear regression, which yields regression yields $\alpha = 0.015$ (see Eq. 5). We find that our theoretical prediction explains $\sim 81\%$ of the variance in the observed melt rates. This suggests that, for ice shelves in which the melt are driven by CDW inflows, variations in these melt rates is accurately accounted for by our geostrophic constraint on the inflow of CDW into the cavity. As expected, the theory does less well at predicting the melt rate in "colder" ice shelves that exhibit lower melt rates, and in which CDW inflows do not dominate the melt rate. Note that in colder ice shelf cavities, the error bars on observations also begin to become equal to the signal in magnitude.

In Fig. 4(d) we use our theory to provide insight into the relative importance of ice draft slope versus external hydrography in setting the observed ice shelf melt rates. Specifically, we map the melt rates in a parameter space defined by two parts of Eq. 6: the cavity-averaged ice shelf slope, $\overline{s_{\mathrm{ice}}}$, and the CDW pressure head (Zhao et al., 2019) multiplied by its temperature anomaly, $\langle H_{\mathrm{CDW}}\rangle\langle g'_{\mathrm{out}}\rangle\langle\theta_{\mathrm{CDW}}-\theta_{\mathrm{surf}}\rangle$. This decomposition shows that ice shelves with similarly high rates of melt may result either from an abundance of warm CDW that has access to the cavity, *e.g.* Dotson ice shelf, or from a relatively steep ice draft, *e.g.* Moscow University ice shelf. Furthermore, neglecting changes in ice shelf slope, the theory predicts that ice shelves with gentle slopes like the eastern Ross ice shelf would exhibit little melt even if CDW was to rise significantly, in contrast to steeply sloping ice shelves like the Totten ice shelf.

## 6 Discussion and Conclusion

This study presents a novel constraint on the heat transport into ice shelf cavities, and thus, indirectly, on the area-averaged melt rates of the ice shelves. The guiding principle of our theory (Section 2) is that CDW inflows are geostrophically constrained by the along-cavity density gradient established by the interface between CDW and meltwater within the cavity. Applying scaling arguments, we obtain a relationship (5) between the area-averaged melt, the slope of the ice shelf draft, and the thickness, temperature and density anomaly of CDW. Motivated by previous findings that the deepest troughs in the continental shelf play a key role in funneling CDW toward ice shelves, (e.g. Walker et al., 2007; St-Laurent et al., 2013) we further introduce a new metric called the Highest Unconnected isoBath that identifies the locations and depths of these troughs (Section 3). We use the HUB to constrain the waters that can access a given ice shelf cavity, which in turn constrains the along-cavity density gradient and thus the heat transport in our theory. We evaluate our theoretical prediction across a suite of idealized model simulations (Section 4), finding that it explains 90% of the variance of the diagnosed melt rates. Finally, we apply the theory to predict observational estimates of ice shelf melt rates (Adusumilli et al., 2020), and find that the theory explains $> 80\%$ of the variance across all Antarctic ice shelves (Section 5). Taken together, these findings indicate that our geostrophic constraint captures the leading-order dynamics of the heat transport into warm Antarctic ice shelf cavities.

Our formulation contrasts from existing parameterizations of ice shelf melt, because rather than focusing on the dynamics of melt once warm water reaches the ice shelf face, ours estimates the transport of heat into the cavity using solely the offshore hydrographic properties and the morphology of the ice shelf and bed. This means that our theory predicts only one area averaged basal melt rate for an ice shelf cavity, and does not produce spatially varying maps of ice shelf melt.

In deriving and applying our theoretical estimate of the heat flux into ice shelf cavities (5) we have made a number of simplifying assumptions, discussed in Section 2. One is that we neglect the effects of wind and surface buoyancy forcing, whereas previous observational and modeling studies indicate that these effects may play a key role in controlling ice shelf melt rates (Webber et al., 2017; Thoma et al., 2008; Hattermann, 2018; Guo et al., 2022; Silvano et al., 2022). We also assume that the cavity circulation is in equilibrium with the external oceanic conditions, *i.e.* that the heat transport into the cavity is completely used for ice shelf melt. We might expect this assumption to fail on time scales shorter than the flushing time scale of the cavity (Holland, 2017), on which transient heat storage in the cavity and ice shelf boundary layer/plume dynamics more directly dictate the melt rate (Lazeroms et al., 2018). Our theory also predicts that the melt rate is entirely determined by the ice shelf geometry and the external hydrography, in contrast with previous studies showing that circulation within ice shelves can exhibit bi-stable states (Hellmer et al., 2017; Moorman et al., 2023; Caillet et al., 2023). Future work is required to reconcile our theory with previous theories for bi-stability of ice shelf cavity circulation and melt rates (Hazel & Stewart, 2020).

To our knowledge, this is the first time satellite-derived melt has been successfully estimated using offshore hydrographic observations without a tuning for every ice shelf. The framework succeeds despite observational error in the bathymetry, hydrographic, and basal melt measurements. We argue this represents a fundamental advance in community understanding of ice shelf cavity dynamics and could lead to improved parameterizations with better predictive capabilities. While the theory is less predictive in colder ice shelves, the ability of the theory to separate shelves with high melt rates due to CDW inflow from those with lower melt rates we believe could be very useful in developing new understanding of melt in those cold ice shelves.

## 7 Open Research

The observational hydrographic data used in this project is available on the National Centers for Environmental Information website (`https://www.ncei.noaa.gov/access/metadata/landing-page/bin/iso?id=gov.noaa.nodc:NCEI-WOA18`). BedMachine version 2 bathymetric and ice shelf thickness data is available from the National Snow and Ice Data Center (`https://nsidc.org/data/nsidc-0756/versions/2`). Antarctic boundaries from satellite radar are available from the NSIDC as well (`https://nsidc.org/data/nsidc-0709/versions/2`). Satellite derived estimates of basal melt from Adusumilli et al. (2020) can be found in the supplementary information (`https://static-content.springer.com/esm/art%3A10.1038%2Fs41561-020-0616-z/MediaObjects/41561_2020_616_MOESM1_ESM.pdf`). The analysis code for the observational work detailed in this paper is freely available on GitHub (`https://github.com/garrettdreyfus/HUB`). The modelling setup and analysis code for the modeling work in this paper is also available on GitHub (`https://github.com/andystew7583/MITgcm_ISC`).

**Acknowledgments**

This material is based in part upon work supported by the National Science Foundation under Grant Numbers OCE-1751386 and OPP-2220968, and by the National Aeronautics and Space Administration ROSES Physical Oceanography program under grant number 80NSSC19K1192. This work used the Extreme Science and Engineering Discovery Environment (XSEDE, Towns et al. (2014)), which is supported by National Science Foundation grant number ACI-1548562. Without implying their endorsement, the authors thank Clara Burgard and Ken Zhao for various discussions that improved this study.

## References

Adusumilli, S., Fricker, H. A., Medley, B., Padman, L., & Siegfried, M. R. (2020). Interannual variations in meltwater input to the Southern Ocean from Antarctic ice shelves. *Nature Geoscience*, *13*(9), 616–620. doi: 10.1038/s41561-020-0616-z

Assmann, K. M., Jenkins, A., Shoosmith, D. R., Walker, D. P., Jacobs, S. S., & Nicholls, K. W. (2013). Variability of Circumpolar Deep Water transport onto the Amundsen Sea Continental shelf through a shelf break trough. *Journal of Geophysical Research: Oceans*, *118*(12), 6603–6620. doi: 10.1002/2013JC008871

Boyer, T. P., Garcia, H. E., Locarnini, R. A., Zweng, M. M., Mishonov, A. V., Reagan, J. R., … Smolyar, I. V. (2018). *World ocean atlas 2018.* NOAA National Centers for Environmental Information.

Burgard, C., Jourdain, N. C., Reese, R., Jenkins, A., & Mathiot, P. (2022). An assessment of basal melt parameterisations for Antarctic ice shelves. *The Cryosphere Discussions*, 1–56. doi: 10.5194/tc-2022-32

Caillet, J., Jourdain, N. C., Mathiot, P., Hellmer, H. H., & Mouginot, J. (2023). Drivers and Reversibility of Abrupt Ocean State Transitions in the Amundsen Sea, Antarctica. *Journal of Geophysical Research: Oceans*, *128*(1), e2022JC018929. doi: 10.1029/2022JC018929

Daae, K., Hattermann, T., Darelius, E., Mueller, R. D., Naughten, K. A., Timmermann, R., & Hellmer, H. H. (2020). Necessary Conditions for Warm Inflow Toward the Filchner Ice Shelf, Weddell Sea. *Geophysical Research Letters*, *47*(22). doi: 10.1029/2020GL089237

De Rydt, J., Holland, P. R., Dutrieux, P., & Jenkins, A. (2014). Geometric and oceanographic controls on melting beneath Pine Island Glacier. *Journal of Geophysical Research: Oceans*, *119*(4), 2420–2438. doi: 10.1002/2013JC009513

Dinniman, M. S., Klinck, J. M., & Smith, W. O. (2011). A model study of Circumpolar Deep Water on the West Antarctic Peninsula and Ross Sea continental shelves. *Deep Sea Research Part II: Topical Studies in Oceanography*, *58*(13), 1508–1523. doi: 10.1016/j.dsr2.2010.11.013

Dotto, T. S., Naveira Garabato, A. C., Wåhlin, A. K., Bacon, S., Holland, P. R., Kimura, S., … Jenkins, A. (2020). Control of the Oceanic Heat Content of the Getz-Dotson Trough, Antarctica, by the Amundsen Sea Low. *Journal of Geophysical Research: Oceans*, *125*(8), e2020JC016113. doi: 10.1029/2020JC016113

Flexas, M. M., Thompson, A. F., Schodlok, M. P., Zhang, H., & Speer, K. (2022). Antarctic Peninsula warming triggers enhanced basal melt rates throughout West Antarctica. *Science Advances*, *8*(32), eabj9134. doi: 10.1126/sciadv.abj9134

Gnanadesikan, A. (1999). A simple predictive model for the structure of the oceanic pycnocline. *Science (New York, N.Y.)*, *283*(5410), 2077–2079. doi: 10.1126/science.283.5410.2077

Guo, Y., Bachman, S., Bryan, F., & Bishop, S. (2022). Increasing Trends in Oceanic Surface Poleward Eddy Heat Flux Observed Over the Past Three Decades. *Geophysical Research Letters*, *49*(16), e2022GL099362. doi: 10.1029/2022GL099362

Haigh, M., Holland, P. R., & Jenkins, A. (2023). The Influence of Bathymetry Over Heat Transport Onto the Amundsen Sea Continental Shelf. *Journal of Geophysical Research: Oceans*, *128*(5), e2022JC019460. doi: 10.1029/2022JC019460

Hattermann, T. (2018). Antarctic Thermocline Dynamics along a Narrow Shelf with Easterly Winds. *Journal of Physical Oceanography*, *48*(10), 2419–2443. doi: 10.1175/JPO-D-18-0064.1

Hazel, J. E., & Stewart, A. L. (2020). Bistability of the Filchner-Ronne Ice Shelf Cavity Circulation and Basal Melt. *Journal of Geophysical Research: Oceans*, *125*(4), e2019JC015848. doi: https://doi.org/10.1029/2019JC015848

Heimbach, P., & Losch, M. (2012). Adjoint sensitivities of sub-ice-shelf melt rates to ocean circulation under the Pine Island Ice Shelf, West Antarctica. *Annals of Glaciology*, *53*(60), 59–69. doi: 10.3189/2012/AoG60A025

Hellmer, H. H., Kauker, F., Timmermann, R., & Hattermann, T. (2017). The Fate of the Southern Weddell Sea Continental Shelf in a Warming Climate. *Journal of Climate*, *30*(12), 4337–4350. doi: 10.1175/JCLI-D-16-0420.1

Holland, P. R. (2017). The Transient Response of Ice Shelf Melting to Ocean Change. *Journal of Physical Oceanography*, *47*(8), 2101–2114. doi: 10.1175/JPO-D-17-0071.1

Holland, P. R., Jenkins, A., & Holland, D. M. (2008). The Response of Ice Shelf Basal Melting to Variations in Ocean Temperature. *Journal of Climate*, *21*(11), 2558–2572. doi: 10.1175/2007JCLI1909.1

Jacobs, S. S., Hellmer, H. H., & Jenkins, A. (1996). Antarctic Ice Sheet melting in the southeast Pacific. *Geophysical Research Letters*, *23*(9), 957–960. doi: 10.1029/96GL00723

Jenkins, A., Dutrieux, P., Jacobs, S. S., McPhail, S. D., Perrett, J. R., Webb, A. T., & White, D. (2010). Observations beneath Pine Island Glacier in West Antarctica and implications for its retreat. *Nature Geoscience*, *3*(7), 468–472. doi: 10.1038/ngeo890

Klinck, J. M., & Dinniman, M. S. (2010). Exchange across the shelf break at high southern latitudes. *Ocean Science*, *6*(2), 513–524. doi: 10.5194/os-6-513-2010

Lazeroms, W. M. J., Jenkins, A., Gudmundsson, G. H., & van de Wal, R. S. W. (2018). Modelling present-day basal melt rates for Antarctic ice shelves using a parametrization of buoyant meltwater plumes. *The Cryosphere*, *12*(1), 49–70. doi: 10.5194/tc-12-49-2018

Little, C. M., Gnanadesikan, A., & Oppenheimer, M. (2009). How ice shelf morphology controls basal melting. *Journal of Geophysical Research: Oceans*, *114*(C12). doi: 10.1029/2008JC005197

Losch, M. (2008). Modeling ice shelf cavities in a z coordinate ocean general circulation model. *Journal of Geophysical Research: Oceans*, *113*(C8). doi: 10.1029/2007JC004368

Marshall, J., Adcroft, A., Hill, C., Perelman, L., & Heisey, C. (1997). A finite-volume, incompressible Navier Stokes model for studies of the ocean on parallel computers. *Journal of Geophysical Research: Oceans*, *102*(C3), 5753–5766. doi: 10.1029/96JC02775

Marshall, J., Hill, C., Perelman, L., & Adcroft, A. (1997). Hydrostatic, quasi-hydrostatic, and nonhydrostatic ocean modeling. *Journal of Geophysical Research: Oceans*, *102*(C3), 5733–5752. doi: 10.1029/96JC02776

Moorman, R., Thompson, A. F., & Wilson, E. A. (2023). Coastal Polynyas Enable Transitions Between High and Low West Antarctic Ice Shelf Melt Rates. *Geophysical Research Letters*, *50*(16), e2023GL104724. doi: 10.1029/2023GL104724

Morlighem, M. (2020). *Measures bedmachine antarctica, version 2.* NASA National Snow and Ice Data Center Distributed Active Archive Center.

Morrison, A. K., Hogg, A. M., England, M. H., & Spence, P. (2020). Warm Circumpolar Deep Water transport toward Antarctica driven by local dense water export in canyons. *Science Advances*, *6*(18), eaav2516. doi: 10.1126/sciadv.aav2516

Nakayama, Y., Manucharyan, G., Zhang, H., Dutrieux, P., Torres, H. S., Klein, P., ... Menemenlis, D. (2019). Pathways of ocean heat towards Pine Island and Thwaites grounding lines. *Scientific Reports*, *9*(1), 16649. doi: 10.1038/s41598-019-53190-6

Nicholls, K. W., Østerhus, S., Makinson, K., Gammelsrød, T., & Fahrbach, E. (2009). Ice-ocean processes over the continental shelf of the southern Weddell Sea, Antarctica: A review. *Reviews of Geophysics*, *47*(3). doi: 10.1029/2007RG000250

Nikurashin, M., & Vallis, G. (2012). A Theory of the Interhemispheric Meridional Overturning Circulation and Associated Stratification. *Journal of Physical Oceanography*, *42*(10), 1652–1667. doi: 10.1175/JPO-D-11-0189.1

Nitsche, F. O., Porter, D., Williams, G., Cougnon, E. A., Fraser, A. D., Correia, R., & Guerrero, R. (2017). Bathymetric control of warm ocean water access along the East Antarctic Margin. *Geophysical Research Letters*, *44*(17), 8936–8944. doi: 10.1002/2017GL074433

Paolo, F. S., Fricker, H. A., & Padman, L. (2015). Volume loss from Antarctic ice shelves is accelerating. *Science*, *348*(6232), 327–331. doi: 10.1126/science.aaa0940

Pelle, T., Morlighem, M., & Bondzio, J. H. (2019). Brief communication: PICOP, a new ocean melt parameterization under ice shelves combining PICO and a plume model. *The Cryosphere*, *13*(3), 1043–1049. doi: 10.5194/tc-13-1043-2019

Pritchard, H. D., Ligtenberg, S. R. M., Fricker, H. A., Vaughan, D. G., van den Broeke, M. R., & Padman, L. (2012). Antarctic ice-sheet loss driven by basal melting of ice shelves. *Nature*, *484*(7395), 502–505. doi: 10.1038/nature10968

Rignot, E., Mouginot, J., Scheuchl, B., van den Broeke, M., van Wessem, M. J., & Morlighem, M. (2019). Four decades of Antarctic Ice Sheet mass balance from 1979–2017. *Proceedings of the National Academy of Sciences*, *116*(4), 1095–1103. doi: 10.1073/pnas.1812883116

Rintoul, S. R., Silvano, A., Pena-Molino, B., van Wijk, E., Rosenberg, M., Greenbaum, J. S., & Blankenship, D. D. (2016). Ocean heat drives rapid basal melt of the Totten Ice Shelf. *Science Advances*, *2*(12), e1601610. doi: 10.1126/sciadv.1601610

Schmidtko, S., Heywood, K. J., Thompson, A. F., & Aoki, S. (2014). Multidecadal warming of Antarctic waters. *Science*, *346*(6214), 1227–1231. doi: 10.1126/science.1256117

Schodlok, M. P., Menemenlis, D., Rignot, E., & Studinger, M. (2012). Sensitivity of the ice-shelf/ocean system to the sub-ice-shelf cavity shape measured by NASA IceBridge in Pine Island Glacier, West Antarctica. *Annals of Glaciology*, *53*(60), 156–162. doi: 10.3189/2012AoG60A073

Shepherd, A., Fricker, H. A., & Farrell, S. L. (2018). Trends and connections across the Antarctic cryosphere. *Nature*, *558*(7709), 223–232. doi: 10.1038/s41586-018-0171-6

Shepherd, A., Wingham, D., & Rignot, E. (2004). Warm ocean is eroding West Antarctic Ice Sheet. *Geophysical Research Letters*, *31*(23). doi: 10.1029/2004GL021106

Silvano, A., Holland, P. R., Naughten, K. A., Dragomir, O., Dutrieux, P., Jenkins, A., … Naveira Garabato, A. C. (2022). Baroclinic Ocean Response to Climate Forcing Regulates Decadal Variability of Ice-Shelf Melting in the Amundsen Sea. *Geophysical Research Letters*, *49*(24), e2022GL100646. doi: 10.1029/2022GL100646

Spence, P., Griffies, S. M., England, M. H., Hogg, A. M., Saenko, O. A., & Jourdain, N. C. (2014). Rapid subsurface warming and circulation changes of Antarctic coastal waters by poleward shifting winds. *Geophysical Research Letters*, *41*(13), 4601–4610. doi: 10.1002/2014GL060613

Stewart, A. L., & Thompson, A. F. (2016). Eddy Generation and Jet Formation via Dense Water Outflows across the Antarctic Continental Slope. *Journal of Physical Oceanography*, *46*(12), 3729–3750. doi: 10.1175/JPO-D-16-0145.1

St-Laurent, P., Klinck, J. M., & Dinniman, M. S. (2013). On the Role of

Coastal Troughs in the Circulation of Warm Circumpolar Deep Water on Antarctic Shelves. *Journal of Physical Oceanography*, *43*(1), 51–64. doi: 10.1175/JPO-D-11-0237.1

Tamsitt, V., England, M. H., Rintoul, S. R., & Morrison, A. K. (2021). Residence Time and Transformation of Warm Circumpolar Deep Water on the Antarctic Continental Shelf. *Geophysical Research Letters*, *48*(20), e2021GL096092. doi: 10.1029/2021GL096092

Thoma, M., Jenkins, A., Holland, D., & Jacobs, S. (2008). Modelling Circumpolar Deep Water intrusions on the Amundsen Sea continental shelf, Antarctica. *Geophysical Research Letters*, *35*(18). doi: 10.1029/2008GL034939

Towns, J., Cockerill, T., Dahan, M., Foster, I., Gaither, K., Grimshaw, A., ... Wilkins-Diehr, N. (2014, Sept). XSEDE: Accelerating scientific discovery. *Computing in Science Engineering*, *16*(5), 62-74. doi: 10.1109/MCSE.2014.80

Walker, D. P., Brandon, M. A., Jenkins, A., Allen, J. T., Dowdeswell, J. A., & Evans, J. (2007). Oceanic heat transport onto the Amundsen Sea shelf through a submarine glacial trough. *Geophysical Research Letters*, *34*(2). doi: 10.1029/2006GL028154

Webber, B. G. M., Heywood, K. J., Stevens, D. P., Dutrieux, P., Abrahamsen, E. P., Jenkins, A., ... Kim, T. W. (2017). Mechanisms driving variability in the ocean forcing of Pine Island Glacier. *Nature Communications*, *8*(1), 14507. doi: 10.1038/ncomms14507

Wåhlin, A. K., Yuan, X., Björk, G., & Nohr, C. (2010). Inflow of Warm Circumpolar Deep Water in the Central Amundsen Shelf. *Journal of Physical Oceanography*, *40*(6), 1427–1434. doi: 10.1175/2010JPO4431.1

Youngs, M. K., Ferrari, R., & Flierl, G. R. (2020). Basin-Width Dependence of Northern Deep Convection. *Geophysical Research Letters*, *47*(15), e2020GL089135. doi: 10.1029/2020GL089135

Zhao, K. X., Stewart, A. L., & McWilliams, J. C. (2019). Sill-Influenced Exchange Flows in Ice Shelf Cavities. *Journal of Physical Oceanography*, *49*(1), 163–191. doi: 10.1175/JPO-D-18-0076.1